nature communications

Article

https://doi.org/10.1038/s41467-025-57615-x

Endocrine-exocrine *miR-503-322* drives aging-associated pancreatitis via targeting MKNK1 in acinar cells

Received: 3 June 2024

Accepted: 23 February 2025

Published online: 17 March 2025

Check for updates

Kerong Liu[1,2], Tingting Lv[1], Lu He[1], Wei Tang[3], Yan Zhang[4], Xiao Xiao[1], Yating Li[1], Xiaoai Chang[1], Shusen Wang[5], Stephen J. Pandol[6] ✉, Ling Li[7] ✉, Xiao Han[1,8] ✉ & Yunxia Zhu[1] ✉

Aging is the risk factor for chronic pancreatitis and severity determinant for its acute attack, yet the underlying cause is unclear. Here, we demonstrate that senescent β-cells of endocrine pancreas decide the onset and severity of chronic and acute pancreatitis. During physiological aging, senescent β-cells increase the expression of *miR-503-322* which is secreted as small extracellular vesicles to enter exocrine acinar cells, driving a causal and reversible role on aging-associated pancreatitis. Mechanistically, *miR-503-322* targets MKNK1 to inhibit acinar-cell secretion leading to autodigestion and repress proliferation causing repair damage of exocrine pancreas. In the elderly population, serum *miR-503* concentration is negatively correlated with amylase, prone to chronic pancreatitis due to increased *miR-503* and decreased MKNK1 in the elderly pancreas. Our findings highlight the *miR-503-322*–MKNK1 axis mediating the endocrine-exocrine regulatory pathway specifically in aged mice and humans. Modulating this axis may provide potential preventive and therapeutic strategies for aging-associated pancreatitis.

Pancreatitis is one of the most common causes of hospitalization worldwide and represents higher prevalence in the elderly[1–3]. Chronic inflammation accumulates during natural aging and has been identified as responsible for the onset of many diseases, including pancreatitis and type 2 diabetes mellitus (T2DM)[4]. Recent clinical data showed that the incidence of pancreatitis increases in patients with T2DM[5–7], indicating the endocrine part of the pancreas participants in pancreatitis formation. However, the underlined mechanisms remain elusive.

The endocrine pancreatic islets have a well-recognized anatomical and physiological integration with the exocrine pancreas and regulate its function[8]. Involvement of the islet-acinar axis (IAA) has been suggested in the islet-acinar portal system for the physiological regulation of acinar cell function by islet peptides[9,10]. A recent study found that islet β-cell-derived cholecystokinin (CCK) acts on acinar cells via the IAA to promote the progression of pancreatic ductal adenocarcinoma (PDAC)[11], suggesting that endocrine islet β-cells can crosstalk with acinar cells. In addition, β-cell inflammation exacerbates pancreatitis through chemokine signaling[12,13]. These findings suggest that factors secreted abnormally by pancreatic β-cells play a key role in the development of pancreatitis. One possibility is that abnormal secretion of microRNAs (miRNAs) may be involved.

[1]Key Laboratory of Human Functional Genomics of Jiangsu Province, Biochemistry and Molecular Biology, Nanjing Medical University, Nanjing, Jiangsu, China. [2]Department of Endocrinology, Affiliated Children's Hospital of Jiangnan University, Wuxi Children's Hospital, Wuxi, Jiangsu, China. [3]Department of Endocrinology, Geriatric Hospital of Nanjing Medical University, Nanjing, Jiangsu, China. [4]Children's Hospital of Nanjing Medical University, Nanjing, Jiangsu, China. [5]Organ Transplant Center, Tianjin First Central Hospital, Nankai University, Tianjin, China. [6]Division of Gastroenterology, Department of Medicine, Cedars-Sinai Medical Center, Los Angeles, CA, USA. [7]Department of Endocrinology, Zhongda Hospital, School of Medicine, Southeast University, Nanjing, Jiangsu, China. [8]Department of Endocrinology, The First Affiliated Hospital of Nanjing Medical University, Nanjing, Jiangsu, China.
✉e-mail: Stephen.Pandol@cshs.org; lingli@seu.edu.cn; hanxiao@njmu.edu.cn; zhuyx@njmu.edu.cn

Pancreatic β-cells are known to mediate intercellular communication through the secretion of extracellular vesicles (EVs) rich in miRNAs, resulting in reduced insulin sensitivity and secretion capacity in a paracrine or distal manner and elevated blood glucose levels[14]. However, a regulatory role for miRNAs carried by EVs derived from β-cells has not been established for pancreatitis. We have previously demonstrated that senescent β-cells released *miR-503-322* as small EVs (~45 nm) which were transported into peripheral target organs to cause insulin resistance, thereby leading to the onset of T2DM[15]. Serendipitously, overexpression of *miR-503* in β cells caused pancreatitis-like changes with age, suggesting that *miR-503* secreted by endocrine β-cells may be important in regulating exocrine functions including pancreatitis.

The X-linked *miR-503*, clustered with *miR-322* has been investigated and shown to play an important role in modulating cell proliferation, cell differentiation, and tissue remodeling[16]. In the present study, we found that during natural aging, primary *miR-503-322* (*Pri-miR-503*) was transcribed in the endocrine islets while mature *miR-503* and *miR-322* could be detected in both endocrine and exocrine pancreas. Increased levels of *miR-503-322* in senescent acinar cells were derived from β-cells and intra-acinar *miR-503-322* promoted pancreatitis by targeting MAP kinase-interacting kinases (MKNK1). The regulation mode was also conserved in aged population, adding further evidence for endocrine-exocrine crosstalk in regulating pancreatitis and providing therapeutic targets for the prevention and treatment of aging-associated pancreatitis.

Results

Senescent β-cell-derived *miR-503-322* promoted pancreatitis in mice

Our previous study showed that β-cell-specific *miR-503* transgenic (βTG) mice suffered from insulin resistance and β-cell dysfunction, leading to T2DM[15]. Coincidentally, we noted that the βTG mice also showed chronic pancreatitis (CP)-like changes with advanced age, including diffuse expansion of the interlobar septae, fat accumulation, and fibrosis (Fig. S1A, B). Adult βTG mice also showed significant exacerbation of caerulein-induced AP attack, as evidenced by pancreatic edema, macrophage infiltration, and more severe histologic scorings compared with the WT mice (Fig. S1C–E).

To understand the role of β-cell *miR-503* on the development of pancreatitis, the expressing distribution of *miR-503* in βTG mice was detected. We found that *Pri-miR-503* was significantly increased in islets but not in acini, while the mature *miR-503* was increased in both islets and acini (Fig. 1A, B), suggesting β-cell *miR-503* entering acinar cells. The same expression profiles of *Pri-miR-503* and mature *miR-503* and *miR-322* were also observed in aged mice (Fig. 1C, D). We previously reported that senescent β-cells secrete *miR-503-322* within EVs[15]. To validate our findings, we measured *miR-503* and *miR-322* (namely *miR-424* in humans) levels in EVs from a 69-year-old human islet donor after senescent cell removal using senolytics ABT263 (Fig. S2A). Previous studies have shown that senescent β-cells can be specifically killed in vitro with ABT263[17]. A 48-hour treatment with ABT263 reduced β-galactosidase-positive cells and p16INK4a fluorescence in insulin-positive β-cells, and consequently, the secretion of *miR-503-424* in EVs was diminished (Fig. S2B–D). These results make us think about the contribution of β-cell *miR-503-322* to pancreatitis in older age. Consistent with our hypothesis, aged mice showed a more severe form of caerulein-induced AP compared to younger mice (Fig. S2E–I), which could be significantly improved by blocking β-cell *miR-503-322* levels. An insulin 2 promoter-driven sponge-AAV (SP-AAV) specifically expressed in β cells resulted in decreased expression levels of *miR-503-322* in pancreas (Fig. 1E–G). Meanwhile, caerulein-induced AP measured by serum amylase and lipase levels, pancreatic edema, histologic scorings were significantly ameliorated in aged mice infected with SP-AAV (Fig. 1H–L). These findings indicate that increased levels of *miR-503-322* in senescent β cells contribute pancreatitis severity associated with older age.

β cell secreted small extracellular vesicles containing *miR-503-322* to enter acinar cells

We previously verified that islet-derived EVs were secreted from insulin granules and were trafficked into liver and adipose tissues via circulation[15]. Whether those EVs entered acinar cells was unknown. Here, we show that acinar cells indiscriminately engulfed EVs in vitro models (Fig. S3A), and acinar cells that received EVs purified from βTG islets had significantly greater levels of *miR-503* than acinar cells that received EVs from wildtype (WT) islets (Fig. S3B). To validate the specificity of β-cells, we used the cell-permeable zinc-selective dye FluoZin™-3, which selectively sorts pancreatic β-cells without compromising their viability or function[18], enabling enrichment of β-cell-derived EVs (βEVs) (Fig. S3C–E). Transmission electron microscopy (TEM) revealed βEVs with a diameter of about 45 nm (Fig. 2A), and nanoparticle tracking analysis (NTA) confirmed size of 42 nm (Fig. 2B). Western blotting confirmed high expression of EV markers (ALIX, TSG101, and CD63), but not GAPDH which was not included in EVs (Fig. 2C). Although the concentration was not different, βEVs released from βTG were found to package more *miR-503* than those from WT β-cells (Fig. 2D, E). The in vitro uptake of βEVs by acinar cells and flow cytometry data showed that acinar cells can internalize βEVs with no significant difference in uptake efficiency (Figs. 2F and S2F–H). Whereas the level of *miR-503* in acinar cells receiving βTG-βEVs was significantly higher than those receiving WT-βEVs (Fig. 2G). We also injected labeled islet-derived EVs into mice via pancreatic ductal infusion and observed that acinar cells indiscriminately engulfed EVs in vivo (Fig. 2H, I).

To avoid the influence of insulin resistance and hyperglycemia in βTG mice[15], we constructed RIP2-cre;*miR-503-322* KI (βKI) mice which were not overtly diabetic (Fig. S3I–L). βKI mice also exhibited an exacerbation of caerulein-induced AP compared to littermate controls (Fig. 2J–L). Thus, we concluded that β-cell-derived small EVs enter acinar cells and drive pancreatitis at a *miR-503-322*–dependent manner in mice.

Elevation of *miR-503-322* in acinar cells triggers both acute and CP

Next, we sought to investigate the effects of *miR-503-322* under inducible global elevation conditions by using CAG-creER;*miR-503-322* KI (CKI). After tamoxifen induction three times, *Pri-miR-503* expression levels were significantly elevated in the pancreas, skeletal muscle and other metabolic tissues (Fig. S4A, B). Surprisingly, CKI mice started to lose weight and activity, culminating in death due to severe AP within 6 days of the first induction, as observed by significantly increased serum amylase and lipase levels, abdominal infiltration of neutrophils and macrophages, and pancreatic saponification, necrosis and histological analysis (Fig. S4C–I). However, no concomitant histological changes were observed in other major abdominal organs (Fig. S4J). Severe AP-induced systemic inflammatory responses were shown by inverted serum ratios of neutrophils and lymphocytes, and elevated serum levels of C-reactive protein (Fig. S4K–M). These results validate that the global overexpression of *miR-503-322* promotes severe AP, indicating the specificity of the *miR-503-322* for pancreas damage.

To rule out the contribution of other tissues, Pdx1-cre;*miR-503-322* KI (heterozygous PKI/WT and homozygous PKI/KI) mice were used to yield high pancreatic-specific expression of *miR-503-322*. The pancreatic *Pri-miR-503* expression was increased in the heterozygous PKI mice (PKI/WT) compared to WT controls and was further increased in the homozygous mice (PKI/KI) (Fig. 3A). The PKI/KI mice showed an unexpected weight loss at ~6 weeks of age, while the PKI/WT mice showed no change during natural growth (Figs. 3B and S5A). The most prominent features of CP, including pancreatic atrophy, fibrosis,

https://doi.org/10.1038/s41467-025-57615-x

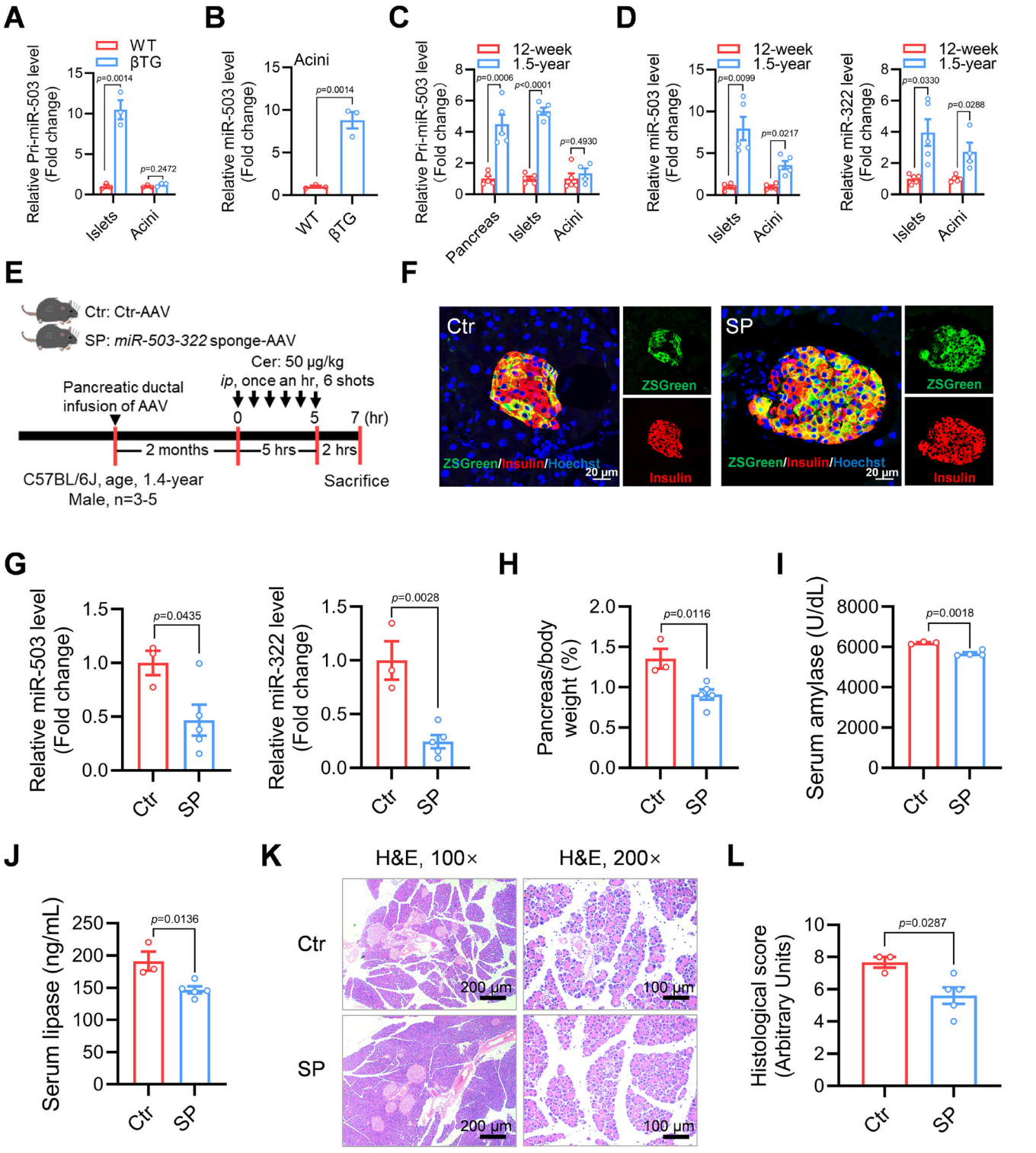

Fig. 1 | Senescent β-cell-derived *miR-503-322* promoted pancreatitis in mice. **A** qPCR analysis of *Pri-miR-503* expression in islets and acini of 20-week-old control (WT) and β-cell-specific *miR-503* transgenic (βTG) male mice. $n = 4$. **B** qPCR analysis of *miR-503* expression in acini of WT and βTG mice. $n = 3$. **C** qPCR analysis of *Pri-miR-503* expression in pancreas, islets and acini of 12 weeks and 1.5 years old male mice. $n = 5$. **D** qPCR analysis of *miR-503* and *miR-322* expression in islets and acini of 12 weeks and 1.5 years old male mice, respectively. $n = 5$. **E** Schematic flow diagram of sponge β-cell *miR-503-322* and induced pancreatitis in aged male mice. The 1.4-years C57BL/6 J male mice were randomly divided into two groups. The control and the experimental group were respectively injected with ctr-AAV and *miR-503–322* sponge-AAV through pancreatic ductal Infusion. Two months later, AP was induced by intraperitoneal injection (i.p.) of caerulein (50 μg/kg, hourly for six consecutive times), and pancreatitis parameters were detected 2 h after the last injection. **F** Representative sections of ZsGreen (green), insulin (red) and nucleus (blue) immunofluorescence co-staining in pancreas of mice 1 month after AAV injection. $n = 3$ mice. **G** qPCR analysis of pancreatic *miR-503* and *miR-322* in the Ctr and SP groups 2 months after AAV injection. Ctr, $n = 3$ and SP, $n = 5$. **H**–**L** Pancreatic weights after calibration with body weight (**H**), serum amylase (**I**), and lipase (**J**), representative histologic sections of H&E of pancreas (**K**), pancreatic histological scores (**L**) in the Ctr and SP groups after caerulein (50 μg/kg) induced. Ctr, $n = 3$ and SP, $n = 5$. Data are means ± SEM. Unpaired Student's *t* tests were used to evaluate statistical significance. Source data are provided as a Source Data file.

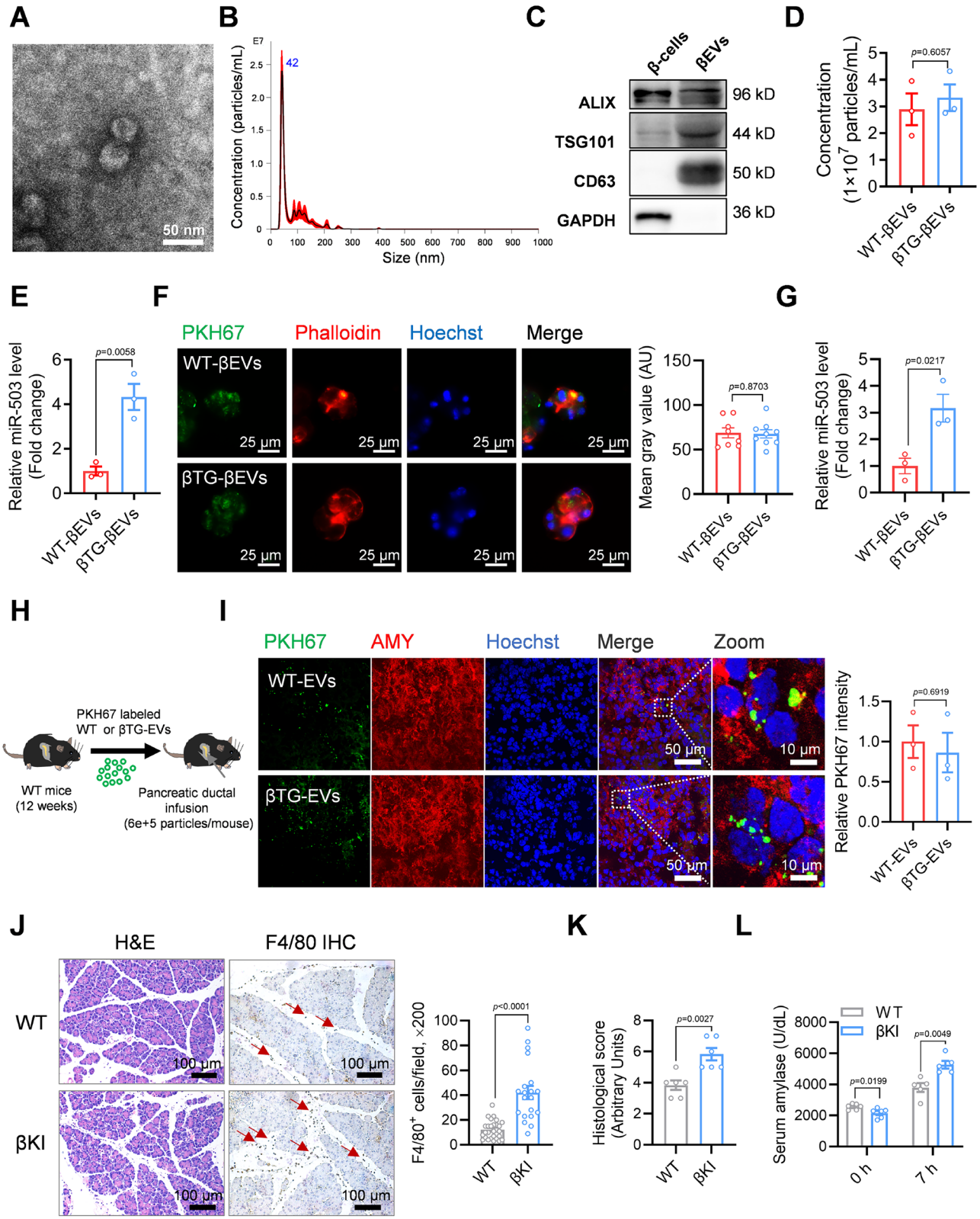

tubular complexes, and inflammatory infiltration were observed in PKI/WT mice, with more severe CP and gross changes in the homozygous PKI/KI mice (Figs. 3C–E and S5B–D). Accordingly, PKI/KI mice could not survive for 12 weeks (Fig. 3F).

PDX1 is a master regulator in pancreas organogenesis while the maturation and identity preservation of islet β-cells and δ-cells[19,20]. To avoid development defect, inducible acini-specific *miR-503-322* (*Elastase*-CreER;*miR-503-322* KI, EKI) mice were also constructed, and overexpression verified post-induction for 3 days (Fig. 3G, H). After tamoxifen injection, the EKI mice showed significantly increased indicators of AP, including macrophage infiltration, tissue damage, and necrosis (Figs. 3J and S5E, F), and had a 50% mortality rate (Fig. 3K). Those mice that survived developed histology of CP one month post-induction, manifested as pancreatic atrophy (Fig. S5G), fibrosis, fat

Fig. 2 | β cells secreted small EVs containing *miR-503-322* to enter acinar cells. **A**–**C** Identification of EVs collected from 20-week-old WT and βTG mouse islet β-cells: TEM images showing the morphology of βEVs collected (A), NTA analysis of nanoparticle size distribution (**B**), and molecular marker identification of βEVs (**C**). $n = 2$ independent experiments. As there was no significant difference between WT and βTG, the results are presented in the figure for βEVs from WT β-cells. **D** NTA analysis of nanoparticle concentration of βEVs collected from 20-week-old WT and βTG mouse islet β-cells. $n = 3$. **E** qPCR analysis of *miR-503* expression in βEVs of WT and TG. $n = 3$. **F** PKH67-labeled WT-βEVs or βTG-βEVs were co-incubated with fresh acini for 8 h. Representative confocal images of PKH67 (green), phalloidin (red), and nuclei (blue) in primary acini and quantification of PKH67 fluorescence intensity. $n = 3$ replicates, with each data point representing a count of 3 acini. **G** qPCR analysis of *miR-503* expression in the acini of received βEVs. $n = 3$ independent experiments. **H**, **I** Experimental scheme: PKH67-labeled WT-EVs or βTG-EVs were infusion into the C57BL/6 J male mouse pancreas via pancreatic ductal. The pancreas was harvested after 12 h, stained with frozen sections for amylase, and then visualized. Representative confocal images of PKH67 (green), amylase (red) and nuclei (blue) of pancreas and quantitation of relative PKH67 fluorescence intensity. $n = 3$ mice. **J**–**L** Pancreatitis parameters assay after initial caerulein (50 μg/kg) injection 7 h in 12-week-old WT and β-cell-specific *miR-503-322* knock-in (βKI) female mice. H&E and F4/80 immunohistochemistry (IHC) of pancreatic sections, quantitation of the number of F4/80 positive cells in pancreatic sections under ×200 microscopic view (J), pancreatic histological scores (**K**) and level of serum amylase (**L**). Arrows indicate the macrophages. $n = 5$ mice. Data are means ± SEM. Unpaired Student's t tests were used to evaluate statistical significance. Source data are provided as a Source Data file.

replacement, and acinar-to-ductal metaplasia (ADM, Fig. 3L, M), while a return to normal levels of serum amylase and lipase (Fig. S5E, F). As shown in Fig. S5H–J, EKI female mice presented an AP phenotype similar to that of male mice 5 days after tamoxifen induction.

The above findings demonstrate that global, pancreatic, and acinar cell-specific overexpression of *miR-503-322* can directly trigger (severe) acute and CP in a dose- and tissue-dependent manner.

MiR-503-322 knockout alleviated caerulein-induced acute pancreatitis

The possibility that ablation of *miR-503-322* could alleviate AP was investigated by the global deletion of *miR-503-322* (KO) (Fig. S6A). The KO mice were viable and fertile, with normal body weight (Fig. S6B). Histology of the pancreas revealed normal pancreatic morphology (Fig. S6C, D). Challenging the KO and WT mice with caerulein or PBS and assessing for AP severity revealed markedly lower pancreatic edema and amylase and lipase levels in the KO group (Fig. 4A–D). Histological examination revealed reduced pancreatic acinar cell damage, less interstitial expansion (indication of edema), and diminished macrophage infiltration in KO mice during the acute AP phase (Fig. 4E–G). To highlight the influence of aging on pancreatitis, 1-year-old KO mice were treated with caerulein. The findings revealed that KO mice experienced a significant alleviation of caerulein-induced AP compared to control mice (Fig. S6E–I). Together, these data demonstrate that the deletion of *miR-503-322* can significantly alleviate caerulein-induced AP.

MiR-503-322 promotes pancreatitis by inhibiting zymogen secretion and acinar cell proliferation

Next, we sought to identify the mechanisms by which *miR-503-322* promotes the development of pancreatitis. TEM images from the pancreas of the PKI/WT mice revealed an increased number of zymogen granules (Fig. S7A). However, the significantly lower transcript levels of pancreatic enzyme-related genes implied that this did not represent an increased production of zymogen in the acinar cells (Fig. S7B) but was possibly an indication of a secretion defect.

Therefore, we isolated acini and assessed their secretory ability in response to caerulein. The amylase release was significantly lower from the PKI cells than from the WT cells (Fig. 5A). The acinar cells from aged mice showed a similar response to that of the PKI cells, with a reduced secretion of pancreatic enzymes (Fig. 5B), in agreement with the results of previous studies[21]. By contrast, the primary acinar cells from the KO mice showed enhanced amylase secretion (Fig. 5C). The defect of enzyme secretion was attributed to the loss of cytoskeleton modulation from tip to basolateral membranes of acinar cells responding to caerulein (Fig. 5D).

Enzyme secretion defects may cause trypsinogen activation. We observed that trypsinogen activation in acini was visualized by using rhodamine 110 (BZiPAR) which revealed a clear enrichment of green fluorescence in PKI cells (Fig. 5E), and serum trypsin activity was enhanced in the PKI mice (Fig. 5F). These findings indicate that *miR-503-322* inhibits pancreatic enzyme secretion and promotes the intracellular accumulation of zymogen. Subsequent zymogen activation in situ may promote pancreas damage of *miR-503-322* elevated mice.

Activation of trypsinogen by lysosomal enzymes after fusion of the lysosome is the classical mode of pancreatic enzyme activation during AP[22,23]. TEM images of the pancreas from PKI mice show morphological signs of this activation, including numerous autophagy vacuoles in the cytoplasm and abundant zymogen granules varying in size and electron density and sometimes fused together to form irregular "lakes" (Fig. S7C). These phenomena suggest a classical activation of intracellular zymogen in the lysosomes of acinar cells that highly express *miR-503-322*. We verified this by inducing pancreatitis in WT and EKI mice by administration of chloroquine, which destroys the acidic environment in autophagic lysosomes (Fig. S7D). The AP phenotype was alleviated in EKI mice treated with chloroquine, as evidenced by a smaller weight loss, reduced serum amylase and lipase levels, and less tissue damage compared to saline-treated control mice, despite a similar pancreas weight (Fig. S7E–J).

AP significantly stimulates the proliferation of acinar cells almost immediately at the point of injury[24]. Not surprisingly, immunofluorescence staining for PCNA revealed a reduction in the numbers of proliferating acinar cells in the mice expressing high levels of the *miR-503-322*, and an increased proliferation of mesenchymal cells (Fig. 5G–I). Conversely, ablation of *miR-503-322* enhanced acinar cell proliferation during the repair phase of caerulein-induced AP (Fig. 5G, J). We also conducted a similar test in aged mice and again observed a significant decrease in acinar cell proliferation similar to that seen in the high *miR-503-322* expression model mice (Fig. 5G, K).

Taken together, these data suggest that *miR-503-322* suppresses zymogen secretion to initiate acute pancreatitis. Meanwhile, *miR-503-322* also inhibits the regenerative proliferation of acinar cells to promote the formation of CP.

MKNK1 is a target of *miR-503-322* and acinar cell-specific restoration of it reverses the phenotype of pancreatitis in mice

We previously used unbiased proteomics to identify target genes of *miR-503* in regulating peripheral insulin resistance and β-cell dysfunction[15]. By analyzing the same proteomics data combined with Targetscan software analysis, five genes (MKNK1, CCNE1, IGF1R, PI3KR1 and INSR) were potential targets (Fig. S8A). After extensively searching and reading literature, we found that the MKNK1, mostly expressed in the exocrine pancreas might contribute to *miR-503-322*–caused pancreatitis. MKNK1 plays an indispensable role in physiological exocrine secretory response[25]. Consistent with published data, phosphorylation of MKNK1 and its downstream eIF4E was increased 4 hr after the first caerulein injection and gradually recovered (Fig. S8B–E). MKNK1 was redistributed to the basolateral region after caerulein administration, assisting acinar cell secretion (Fig. S8F). Previous studies showed that

https://doi.org/10.1038/s41467-025-57615-x

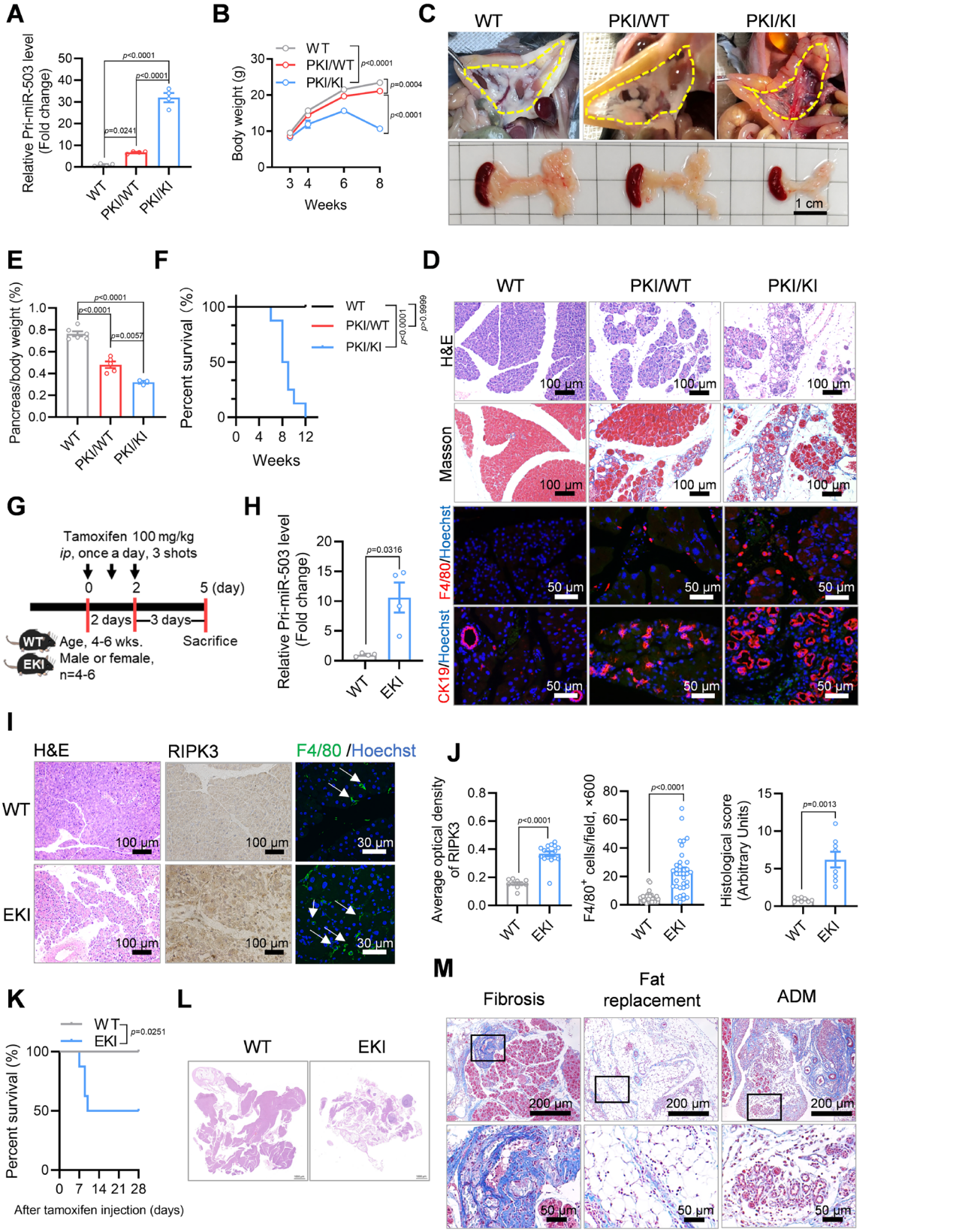

ablation of MKNK1 results in exacerbation of pancreatitis caused by caerulein due to defects of zymogen secretion and acinar cell proliferative in mice[25], making us pursue the role of MKNK1 as a target gene of *miR-503-322*.

Our proteomics analysis showed a decrease in MKNK1 after *miR-503* elevation. Dual-luciferase assay confirmed the regulatory role of *miR-503-322* on the 3'UTR of *Mknk1* gene (Figs. 6A and S9A, B). Next, immunohistochemistry staining of pancreas sections revealed clear suppression of MKNK1 protein amount in the three *miR-503-322* overexpressing mouse model. (Fig. S9C), while upregulation of MKNK1 was induced by caerulein in KO mice (Fig. S9D). The protein levels of MKNK1 and its associated P-MKNK1/P-eIF4E signaling were significantly reduced

https://doi.org/10.1038/s41467-025-57615-x

Fig. 3 | Direct elevation of *miR-503-322* triggers both acute and chronic pancreatitis. A qPCR analysis for pancreatic *Pri-miR-503* expression in 8-week-old control (WT), PKI heterozygous (PKI/WT) and PKI homozygous (PKI/KI) male mice. $n = 5$. **B** Weight monitoring in WT, PKI/WT and PKI/KI male mice. $n = 4$. **C**, **D** Photograph of the pancreas (**C**), representative sections of of H&E, Masson, F4/80 and CK19 immunofluorescence staining in pancreas of 8-week-old PKI male mice (**D**). $n = 3$ mice. **E** Pancreatic weights after calibration with body weight in 8-week-old PKI male mice. WT, $n = 6$; PKI/WT, $n = 5$; PKI/KI, $n = 3$. **F** Survival curves for WT, PKI/WT and PKI/KI male mice. **G** Schematic of acinar cell-specific miR-503-322 knock-in (EKI) mice: 6–8 weeks WT and EKI male or female mice were injected intraperitoneally (*ip.*) with tamoxifen solution, 100 mg/kg, in corn oil, for three consecutive days and sacrificed 3 days after the last tamoxifen injection. **H** qPCR analysis of *Pri-miR-503* in acinar cells of WT and EKI male mice after three times tamoxifen-induced. $n = 4$. **I** Representative sections of pancreas of H&E, receptor-interacting serine-threonine kinase 3 (RIPK3) immunohistochemistry and immunofluorescence staining of F4/80 after first tamoxifen injection 5 days in WT and EKI male mice. Arrows indicate the macrophages. $n = 4$ mice. **J** Pancreatic histological scores, quantitation of average optical density of RIPK3 and the number of F4/80 positive cells in pancreatic sections under ×600 microscopic view for **I**. $n = 5$ mice, and at least 10 photographs were taken for statistical analysis. **K** Survival curves for WT and EKI male and female mice. **L** Pancreatic H&E of WT and EKI female mice after first tamoxifen injection 28 days. **M** Representative sections of pancreatic Masson dyeing from EKI male mice after first tamoxifen injection 28 days. ADM, Acinar-to-ductal metaplasia. $n = 4$ mice. Data are means ± SEM. Data were analyzed using one-way ANOVA (**A**, **E**), two-way ANOVA with Tukey test (**B**), unpaired Student's *t* tests (**H**, **J**) or Survival cure analyses (**F**, **K**). Source data are provided as a Source Data file.

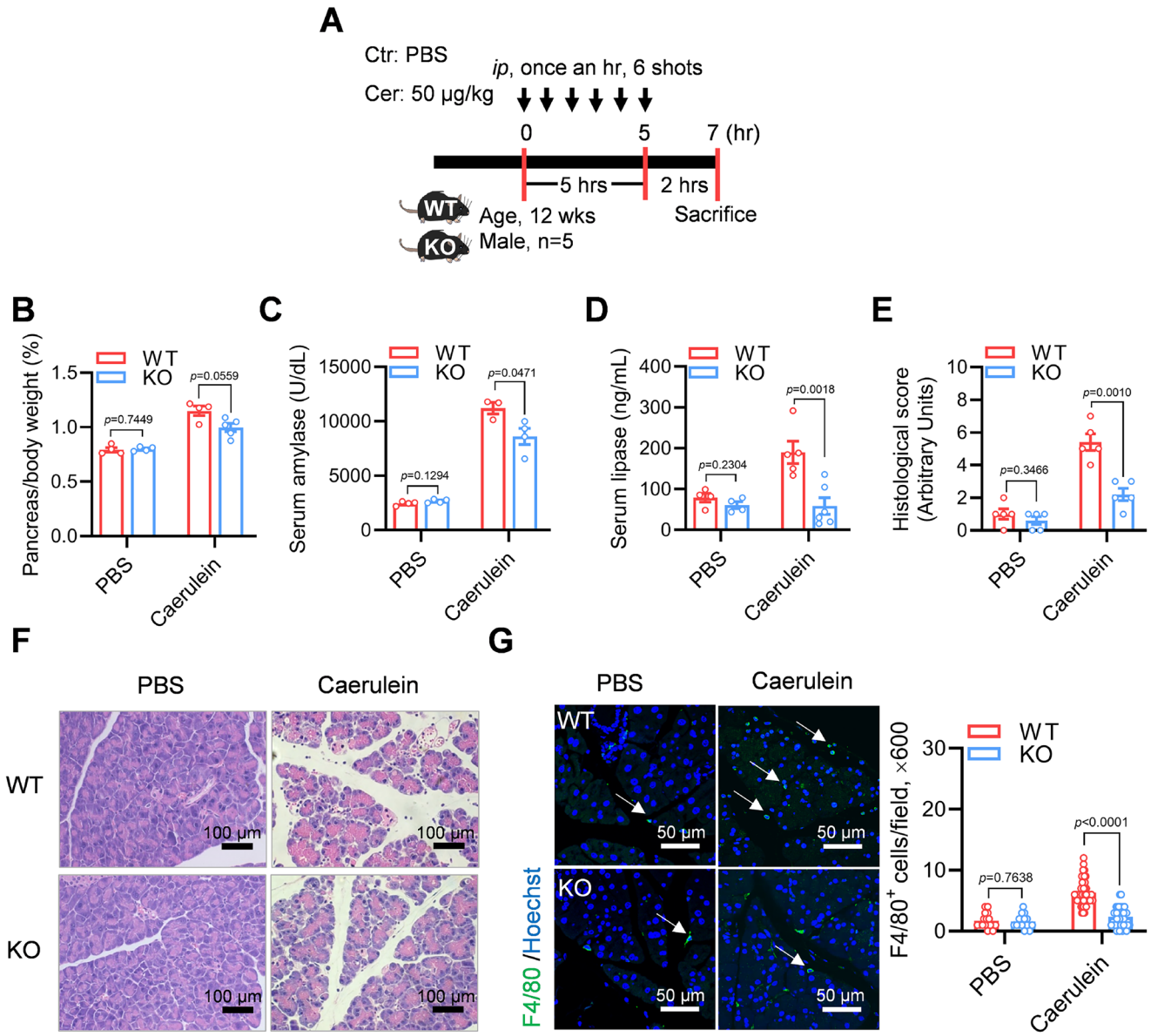

Fig. 4 | MiR-503-322 knockout alleviated caerulein-induced acute pancreatitis. A Schematic of caerulien-induced AP on 12-week WT and KO male mice. **B**–**E** Pancreatic weights after calibration with body weight (**B**), serum amylase (**C**) and lipase (**D**) levels, histological score of the pancreas (**E**) after PBS or caerulein treatment groups. $n = 5$. **F**, **G** Representative sections of pancreatic H&E (**F**) and immunofluorescence staining of F4/80 (green) after PBS or caerulein treatment 7 h in WT and KO male mice. Quantitation of the number of F4/80 positive cells in pancreatic sections under ×600 microscopic view (**G**). $n = 5$ mice, and a total of 30 photographs were taken for statistical analysis. Arrows indicate the macrophages. Data are means ± SEM. Unpaired Student's *t* tests were used to evaluate statistical significance. Source data are provided as a Source Data file.

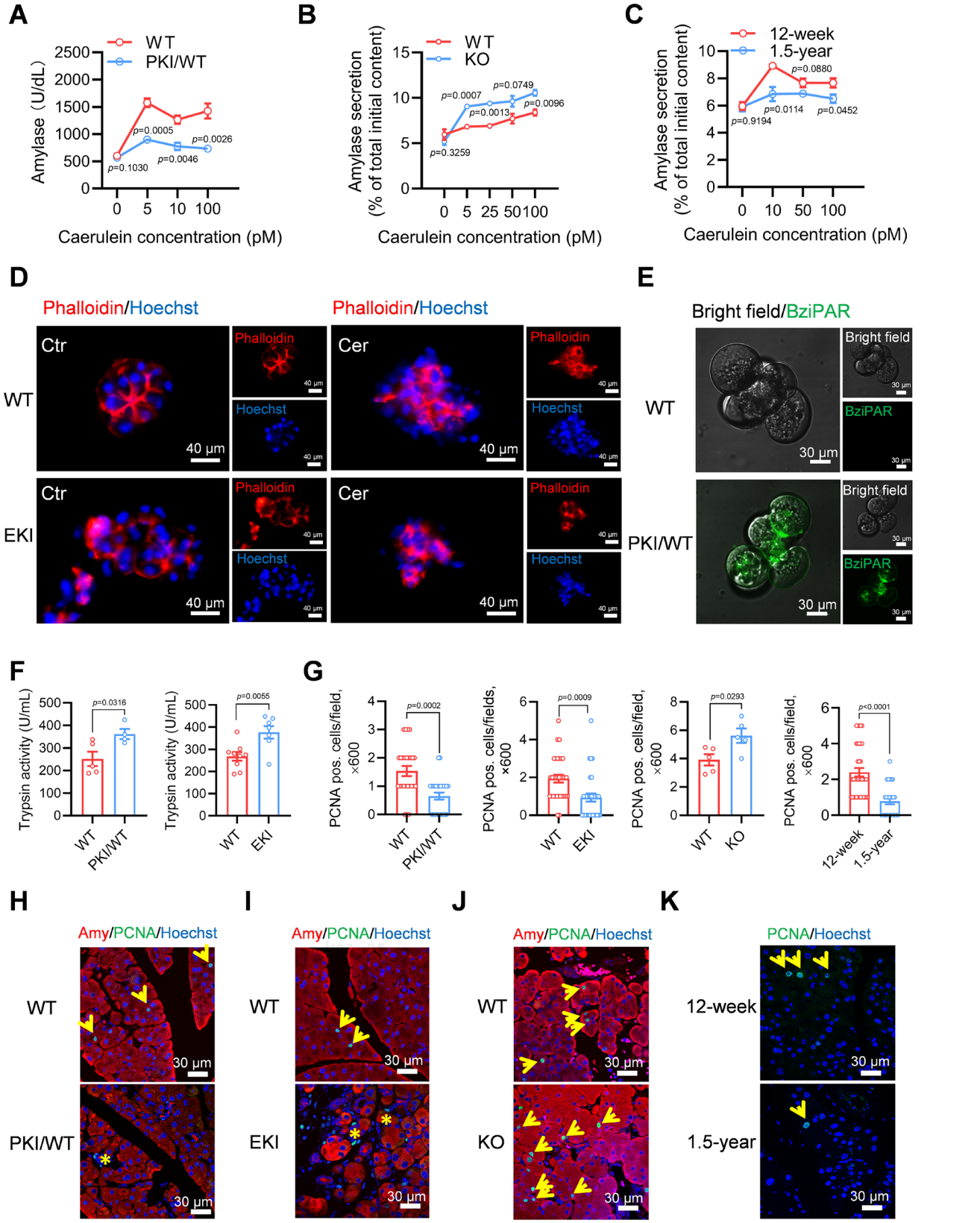

in the pancreas of *miR-503-322* overexpressing model mice and aged mice, and by contrast increased in pancreas of *miR-503-322* knockout mice and aged mice with β-cell-specific blocking *miR-503-322* (Figs. 6B and S9E–G). Taken together, these findings suggest that *miR-503-322* targets MKNK1-eIF4E pathway to inhibit zymogen secretion and acinar cell proliferation, thereby leading to acute and CP.

Next, we tested whether reconstitution of MKNK1 in pancreas could reverse pancreatitis of EKI mice following the schematic diagram (Fig. 6C). We generated an AAV, serotype pancreas (MKNK1-AAV) that directs specific MKNK1 overexpression in the exocrine pancreas. As shown in Fig. S9H, MKNK1 was highly expressed in the acini, but not in the islets of MKNK1-AAV mice. Restoration of MKNK1 also rescued the

Fig. 5 | *MiR-503-322* promotes pancreatitis by inhibiting zymogen secretion and acinar cell proliferation. A Extraction of fresh acinar cells from 8-week-old WT and PKI/WT male mice, in vitro stimulation with caerulein for 30 min and determination of amylase content in the supernatant. $n = 3$. **B**, **C** Amylase levels after calibration of total content release from acinar cells of 12-week WT and KO male mice (**B**) and 12-week and 1.5-year C57BL/6 J male mice (**C**) after 30 min of stimulation with caerulein. $n = 3$. **D** Pancreatic acini from WT or EKI mice, after 48 h tamoxifen induction, were incubated with or without caerulein (0.01 μM) for 30 min. Cells were then harvested, stained for F-actin (red) and nuclei (blue), and imaged by laser confocal microscopy. Micrographs of untreated and caerulein-pretreated acini are shown. $n = 3$ independent experiments. **E** Representative confocal images of WT and PKI/WT male mice acini after incubation with BziPAR for 30 min at 37 °C. $n = 3$ independent experiments. **F** Detection of serum trypsin activity levels in 16-week WT and PKI/WT male mice and EKI after Tamoxifen injection 5 days. $n = 5$. **G** Quantitation of the number of proliferating acinar cells of 8-week WT and PKI/WT male mice; 28 days after tamoxifen induction in WT and EKI male mice; 4 days after caerulein-induced AP in 12-week WT and KO male mice and 12-week and 1.5-year-old male mice. $n = 3$–5 mice per group. $n = 5$ mice. **H**–**J** Representative sections of immunofluorescence staining of amylase (red) and proliferating cell nuclear antigen (PCNA) (green) in pancreatic sections from 8-week WT and PKI/WT male mice (**H**), 28 days after tamoxifen induction in WT and EKI male mice (**I**), 4 days after caerulein-induced AP in 12-week WT and KO male mice (**J**). Arrows indicate proliferating acinar cells; asterisks are proliferating interstitial cells. $n = 5$ mice. **K** Representative sections of immunofluorescence staining of PCNA (green) in pancreatic sections from 12-week and 1.5-year-old male mice. $n = 5$ mice. Arrows indicate proliferating acinar cells. Data are means ± SEM. Unpaired Student's *t* tests were used to evaluate statistical significance. Source data are provided as a Source Data file.

miR-503-322-suppressive protein levels of phos-MKNK1 and phos-eIF4E in the EKI pancreas (Fig. 6D, E). Consequently, MKNK1-AAV-infected EKI mice showed lessened AP phenotypes compared to Ctr-AAV-infected EKI mice. In detail, the loss of body weight, increased serum levels of amylase and lipase, increased number of macrophage infiltration, and tissue damage in Ctr-AAV infected EKI mice were largely reduced in MKNK1-AAV infected EKI mice (Fig. 6F–H).

On the other hand, inhibition of MKNK1 by a verified inhibitor, CGP 57380 further exacerbated caerulein-caused AP phenotypes, and totally erased *miR-503-322* knockout driven protective effects (Fig. S10A–G). These results from acinar cell MKNK1 reconstitution and specific MKNK1 inhibitor support our view that the deficiency of MKNK1 in acini is primarily responsible for the pancreatitis observed in *miR-503-322* elevated mice.

Evidence of *miR-503* and MKNK1 in aging-associated pancreatitis changes in the Chinese population

As the expression of *miR-503* is specifically increased in senescent β cells in mice, we also considered its change in humans. Pancreas sections from elderly adults (EA) showed CP-like changes, including atrophy of the acinar cells, interstitial expansion, and a marked increase in fibrosis (Fig. 7A), as well as a significant reduction in the proportion of proliferating acinar cells (Fig. 7B), compared to that from young adults (YA). Intriguingly, miRNA in situ hybridization showed greater expression of *miR-503* in islets than in acini in pancreatic sections from EA group (Fig. 7C), whereas expression of *miR-503* was almost undetectable in YA group (Fig. 7C). The expression of MKNK1 was significantly downregulated in the acini from the EA pancreas compared to that from the YA pancreas (Fig. 7D). Moreover, the co-localization of MKNK1 and AMY1 in the young acini was dislocated in the elderly acini (Fig. 7D), indicating activation of MKNK1 in the EA. Thus, the increased level of *miR-503* in the acini may come from the islet β cells and contribute to the decreased but activated MKNK1 protein in the elderly Chinese population.

Numerous studies have reported that exocrine pancreas function is impaired in both healthy and diabetic older adults independent of gastrointestinal disease, judged by serum levels of amylase and maximum bicarbonate concentration[26,27]. Consistently, we observed a significantly decreased level of serum amylase in the EA with T2DM (EA + DM) compared to that in YA, moreover, the EAs also showed a decreased amylase level (Fig. 7E). Further analysis showed that serum concentration of *miR-503* in EVs was elevated in the elderly compared to that in the YAs and was further elevated in the EA + DM (Fig. 7F). The human subjects displayed negative associations of serum amylase levels with both age and serum concentrations of *miR-503* in EVs (Fig. 7G, H). These results support the pancreatic exocrine insufficiency in elderly and diabetic patients and point out serum concentrations of *miR-503* in EVs as a molecular marker of ageing-associated pancreatitis in the Chinese population.

Discussion

In this study, we demonstrated that *miR-503-322* derived from endocrine β-cells promotes aging-associated pancreatitis by targeting MKNK1 in exocrine acinar cells. *miR-503-322*, which is produced by senescent β-cells, had an in situ effect in acinar cells that inhibits zymogen secretion and regenerative proliferation. Thus, the *miR-503-322*–MKNK1 axis caused pancreas autodigestion and repairing damage, leading to the onset of acute and CP in mice. This discovery provides an epigenetic mechanism for pancreatitis and adds to the existing evidence of crosstalk between pancreatic endocrine and exocrine.

Gallstones and excessive alcohol use are known to be the major causes of AP in the clinic. Our study identified *miR-503-322* derived from senescent β-cells as a factor that complements traditional etiologies of pancreatitis. Evidence suggests that insulin resistance and diabetes also play roles in pancreatitis[28,29]. *MiR-503-322* secreted by senescent β cells contributes to pancreatitis, independent of insulin resistance and diabetes, as shown by increased severity of caerulein-induced AP in βKI mice prior to hyperglycemia and insulin resistance. However, in conditions of insulin resistance and diabetes, *miR-503-322* exacerbates the severity of pancreatitis, as evidenced by the pancreas-specific knock-in heterozygous and homozygous mice with concomitant exacerbation of diabetes and a more severe pancreatitis phenotype. Previous studies have noted that patients with diabetes develop exocrine dysfunction without obvious symptoms or abnormalities of the pancreatic ducts, termed diabetic pancreatic exocrine disease (DEP)[30,31]. Several hypotheses have been proposed to explain the features of DEP[32–35]. However, none of these concepts are sufficient to explain all the pathological findings. Our previous results showed a significant upregulation of islet *miR-503* expression in patients with T2DM[15]. Suggested by our current investigation, the expressed *miR-503* can then enter and accumulate in the exocrine acini, where it triggers damage to some of the acinar cells and causes CP-like changes in the exocrine pancreas due to repeated pancreas damage.

Most studies report higher overall morbidity and mortality from pancreatitis in the elderly[1], and several explanations for this phenomenon have been put forward[36,37]. The present results confirmed that β-cell-derived *miR-503-322* promotes both acute and chronic damage in the exocrine pancreas and increases mouse mortality with acute and high *miR-503-322* expression (CKI and PKI/KI mice). Therefore, *miR-503-322* may be a common pathogenic factor that can explain the higher morbidity and mortality from pancreatitis in the elderly. Histologically, focal fibrosis also appears to be common in the pancreas of the elderly[38,39]. This is consistent with the observations in human pancreatic sections in the present study. Clinical studies have

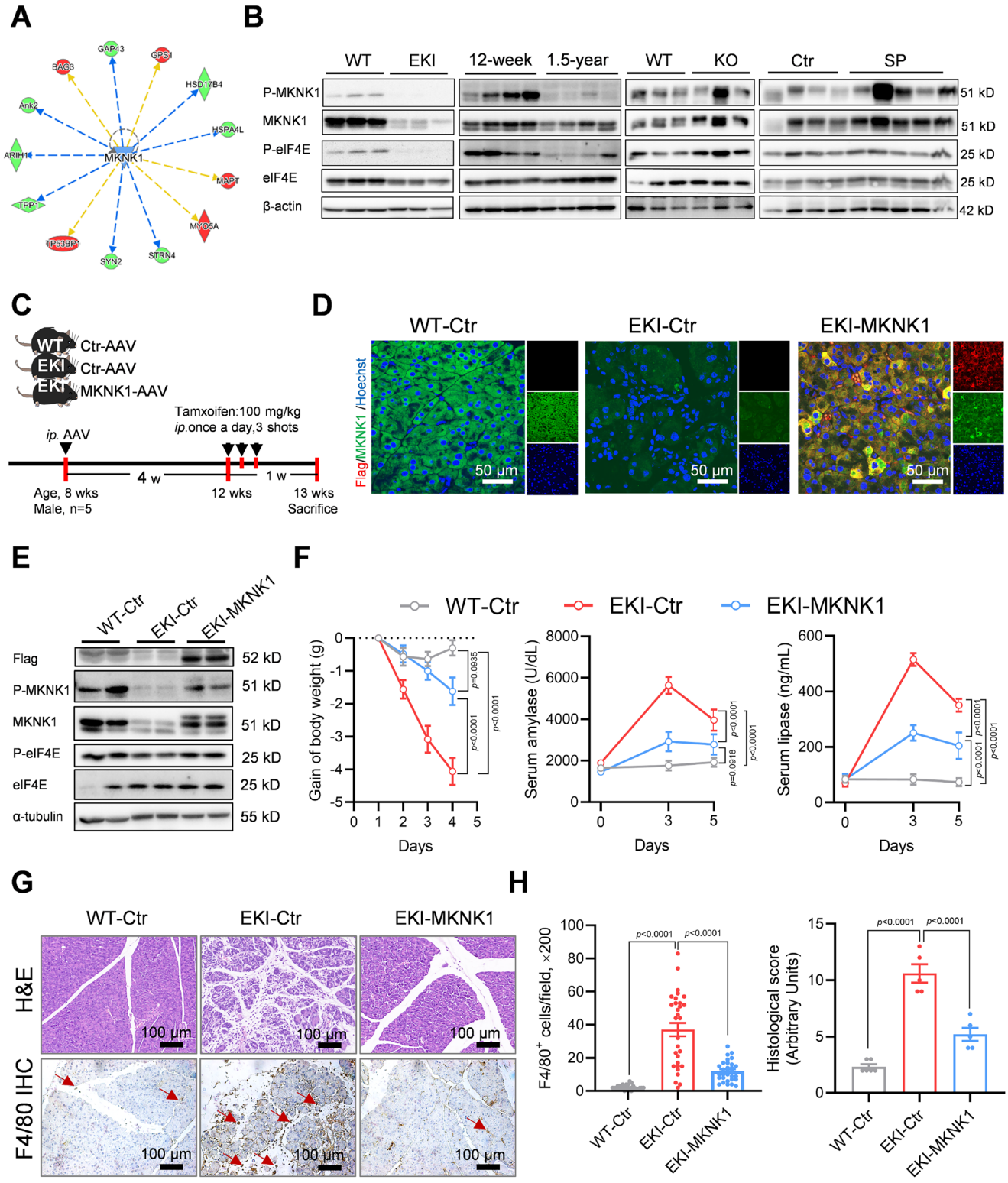

indicated that pancreatic exocrine function is impaired in healthy older individuals without any gastrointestinal disease[40]. The human subjects displayed negative associations of serum amylase levels with both age and serum concentrations of *miR-503*. These results support pancreatic exocrine insufficiency in the elderly and diabetic patients. In our study, we found that *miR-503* inhibits pancreatic enzyme secretion in acinar cells by targeting MKNK1. Decreased MKNK1 expression resulted in dysregulated cytoskeletal remodeling, thus defective movement of zymogen granules from tip to basolateral membrane, which ended up with enzyme secretion defect. Secretion of pancreatic enzyme inhibition with upregulation of *miR-503* expression in normal elderly individuals manifests as lower serum amylase levels. However, it is crucial to note that this secretory blockage can precipitate the accumulation of digestive enzymes in acinar cells, which ultimately results in autodigestion, causing cellular damage and acute attack. In such cases, a transient yet significant release of large quantities of amylase into the serum resulted in a temporary elevation of serum amylase levels. We propose that serum

Fig. 6 | MKNK1 is a target of *miR-503-322* and acinar cell-specific restoration of it reverses the phenotype of pancreatitis in mice. A The MKNK1 network was predicted based on the common signature from the Ingenuity database overlaid with microarray data from *miR-503*-overexpressing mouse pancreatic β cell line MIN6 cells with a 1.5-fold change cutoff compared with negative control cells. **B** WT and EKI male mice at 5 days after tamoxifen induction; Male C57BL/6 J at 12-week and 1.5-year; male WT and KO at 12-week after AP induced and β-cell-specific sponge of *miR-503-322* in control and experimental mice pancreatic protein western blotting. $n = 3–5$. **C** Experimental scheme: 8-week-old WT male mice were injected intraperitoneally (i.p.) with control AAV and EKI male mice were injected with control (Ctr-AAV) and MKNK1-AAV, respectively, one-month later tamoxifen was induced for 3 consecutive days and tested at day 7. $n = 5$. **D** Immunofluorescence staining of Flag (red) and MKNK1 (green) of pancreas sections from each group of mice at 13 weeks. $n = 5$ mice. **E** Western blotting of pancreatic proteins from each group of mice at 13 weeks. $n = 2$. **F** Gain of body weight, serum amylase and lipase level were monitored during tamoxifen induction. $n = 5$. **G** Representative images of H&E and F4/80 immunohistochemistry of the pancreas in each group. Arrows indicate the macrophages. **H** Quantitation of the number of F4/80 positive cells in each group and the pancreatic histological score. $n = 5$ mice, three sections per mouse (50 μm apart), and at least 10 microscopic fields per section. Data are means ± SEM. Data were analyzed using two-way ANOVA (**F**) and one-way ANOVA (**H**) with the Tukey test. Source data are provided as a Source Data file.

amylase levels are elevated in elderly patients during acute attacks, despite the upregulation of *miR-503*. Although the correlations of tissue and serum *miR-503-322* and MKNK1 expression in the aging human population may not necessarily validate the proposed mechanisms and functions observed in transgenic mice, these findings provide valuable clues for further studies of aging-associated pancreatitis.

In humans, AP and CP are diagnosed based on well-defined criteria[41,42]. In mouse models of pancreatitis, while classic symptoms like upper epigastric pain and vomiting are absent, affected mice may show reduced activity and weight loss. Diagnosis relies on increased plasma pancreatic enzyme levels, particularly amylase and lipase, and the pathological features of pancreatic tissue. In our study, global *miR-503-322* overexpressing mice showed increased serum amylase and lipase on day two, with amylase normalizing by day five and lipase remaining elevated. Acinar cell-specific *miR-503-322* knock-in mice exhibited significant enzyme upregulation on day three, with no further changes or decreases. Pancreatic pathology, quantified using a scoring system described by Schmidt et al. is essential for diagnosis[43]. Human pancreatitis follows a course of acute attacks, interventions, and recurrent attacks, ultimately leading to CP[42]. In mouse models, some mice die without prompt treatment, whereas survivors develop CP. The timescale of pancreatitis was more distinct in the inducible acini-specific miR-503-322 knock-in mouse model. AP was significantly detected two days after tamoxifen injection, with a 50% mortality rate. Mice that survived developed histology of CP one-month post-induction, manifested as pancreatic atrophy, fibrosis, fat replacement, and acinar-to-ductal metaplasia, while returning to normal levels of serum amylase and lipase. Despite the morphology of a human pancreas and timescale of developing pancreatitis making it difficult to discern acute and CP in a mouse model, we differentiated AP and CP in mice through serum enzymes and pancreatic pathology.

In healthy adults, *miR-503-322* is expressed mainly in lung, heart, and skeletal muscle progenitor cells[44]. Upregulation of *miR-503-322* occurs in aging acinar cells and is likely to arise from pancreatic β-cells, based on our present observations. Our evidence for this is that blocking *miR-503-322* in islet β-cells of aging mice alleviated caerulein-induced pancreatitis. Our previous findings revealed that *miR-503* from pancreatic islet β-cells reaches the liver and adipose tissue in the form of exosomes, which are known to transport biologically active proteins and miRNAs in their active forms to neighboring cells or distant organs[45–47]. Thus, the involvement of EVs in inter-organ and intra-organ crosstalk has been increasingly studied[48,49]. EVs derived from mesenchymal stem cells have been reported as a treatment for AP by delivering mitochondria and anti-inflammatory factors[50,51]. In addition, senescent β cells have been reported to secrete senescence-associated secretory phenotypes that are rich in EVs and cause dysfunction of adjacent cells through paracrine effects[52,53]. The reported anatomical characteristics of an IAA permit the access of high concentrations of islet-derived *miR-503-322* to exocrine cells. Indeed, a recent study has determined that islet CCK can promote *Kras*-driven PDAC development of an endocrine exchange signal other than insulin[11], supporting the existence of endocrine-exocrine crosstalk via IAA. Therefore, we hypothesize that islet-derived *miR-503-322* is transferred via EVs and the IAA into acinar cells.

Our results support MKNK1 as a *miR-503-322* target gene for the development of pancreatitis. However, MKNK1-knockout mice showed normal pancreatic histology[25], which was inconsistent with the phenotype of AP induced by *miR-503-322*. This normal histologic may reflect the presence of other compensatory pathways in MKNK1-knockout mice as the use of a global mouse model. Indeed, the knockout of MKNK1 adds to the growing list of proteins that have a protective role during AP[54], whereas the acute induction of *miR-503-322* lacks an effective compensatory mechanism. Alternatively, other target genes of *miR-503-322* co-regulating the development of pancreatitis may exist. Moreover, EVs carrying *miR-503-322* may function through inter-organ crosstalk to regulate the severity of AP as shown in CKI mice. In addition, tamoxifen administration occasionally causes pancreatitis also reminded us that the effect of tamoxifen itself cannot be ignored, although it was added to the control group[55]. The mechanisms involved in these possibilities need to be unraveled in further studies.

In conclusion, we demonstrate the role and mechanism of action for pancreatic endocrine-derived *miR-503-322* in promoting pancreatitis in the elderly. Blocking *miR-503-322* in β-cells of aged mice showed good inhibitory effects on pancreatitis, revealing *miR-503-322* as a potential therapeutic target for elderly patients with pancreatitis.

Methods

Human biospecimen acquisition

For human pancreas sections and islets study, conducted in Organ Transplant Center, Tianjin First Central Hospital, Nankai University, Tianjin, China. A total of 20 healthy individuals were recruited, of these, 10 were YA (18–25 years old) and 10 were the EA (60–85 years old) for human pancreas sections. Human islet donor from an elderly person. Islets were digested into single cells with 0.25% trypsin-EDTA (Gibco, USA) and treated with ABT263 (5 μM) (MCE, China) for 48 h, followed by a change to the fresh culture medium. After 24 h, EVs were enriched in the supernatant, and the cells were stained with β-galactosidase (Beyotime, China). Quantification was performed with three replicates per group, at least 15 microscopic fields per well, and a minimum count of 1000 cells. The detailed information of donors was listed in Table S1. Informed consent was obtained from all patients, and the research protocol was reviewed and approved by the research ethics committee of Tianjin First Central Hospital (No. 2018N112KY).

For blood sample collection, conducted in the Department of Endocrinology, Geriatric Hospital of Nanjing Medical University, Nanjing, China, 160 individuals were recruited, including 65 YA (18-55 years old), 65 EA (60-85 years old), and 30 EA with T2DM (EA + DM). Fasting blood samples, collected from all participants, were centrifuged at 850 × *g* for 20 min to separate sera and blood cells, the sera were used for *miR-503* concentration analysis. Detailed information about donors, including age range, fasting blood glucose levels, and history of prior diseases, was listed in Table S2. The study was approved by the research ethics committee of Nanjing Medical University (2022006), and all the volunteers gave written informed consent.

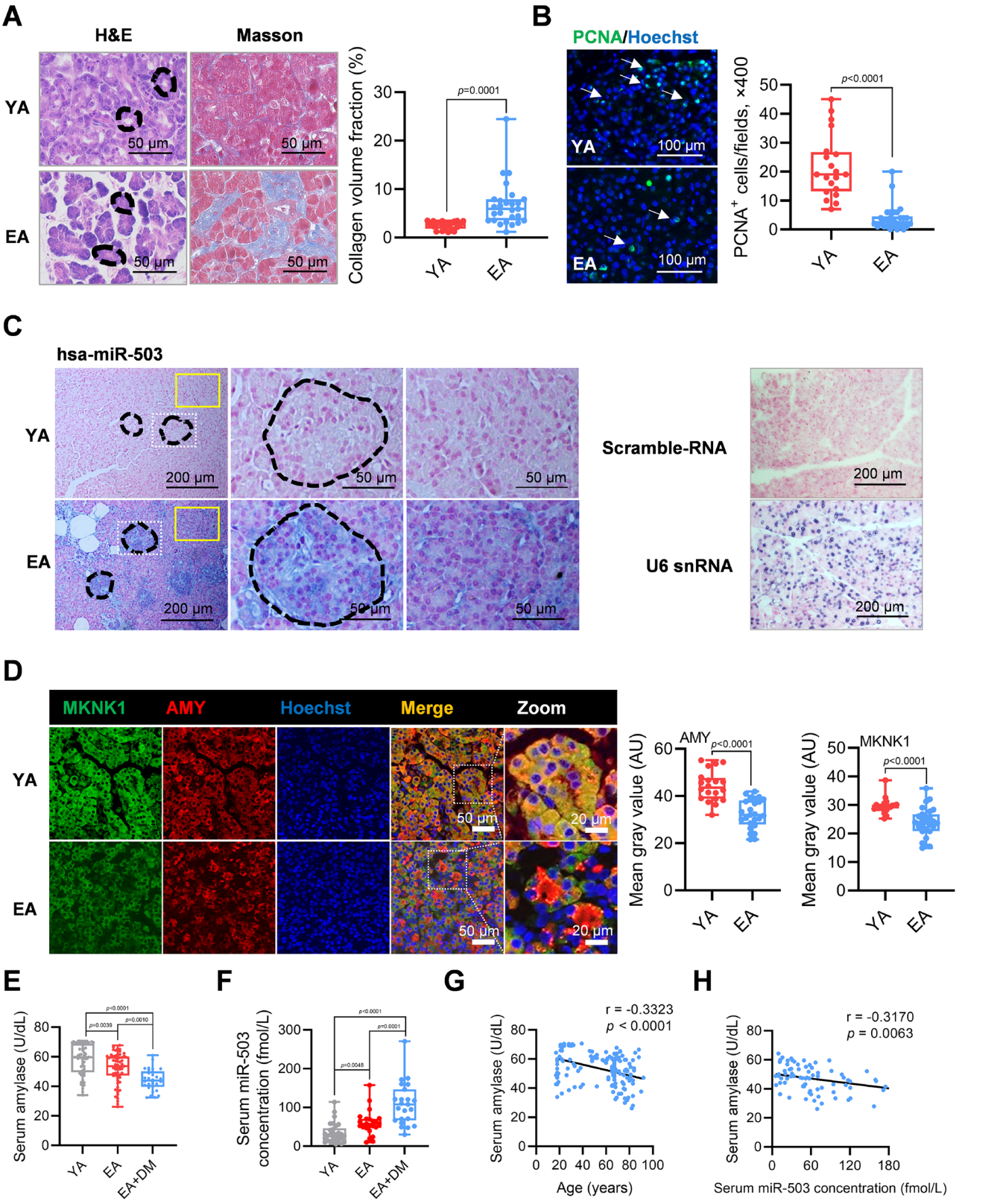

Animal studies

Animal studies were approved by the Research Animal Care Committee of Nanjing Medical University (IACUC-1707023 and IACUC-2004040). Generation of the mouse *miR-503-322* knock-in mouse (H11-CAG-LSL-*miR-503-322* Cas9-KI) by CRISPR/Cas9 was outsourced to GemPharmatech Co, Ltd. The mice were created on the C57BL/6 J genetic background. The gRNA (5′- CTGAGCCAACAGTGGTAGTA -3′) to the Hipp11 (H11) locus, the donor vector containing the "CAG-loxP-Stop-loxP-mouse *miR-503-322*-polyA" cassette, and Cas9 mRNA were co-injected into fertilized mouse eggs to generate targeted conditional knock-in offspring. Rat *insulin 2* promoter (*RIP2*)-Cre (JAX:003573), *CAG*-CreER (JAX:004453) and *PDX1*-Cre (JAX:014647) mice were

Fig. 7 | Evidence of *miR-503* and MKNK1 in aging-associated pancreatitis changes in the Chinese population. A Representative images of H&E and Masson staining of pancreatic sections from the young adult (YA) and the elderly adult (EA); quantitation of collagen volume fraction. The dashed area indicates acini. $n = 10$ and a total of 30 photographs were taken for statistical analysis. **B** Representative images of immunofluorescence staining of PCNA (green) in pancreatic sections and counted the number of PCNA-positive cells. $n = 10$. Arrows indicate proliferating acinar cells. $n = 10$ and a total of 30 photographs were taken for statistical analysis. **C** In situ hybridization of *miR-503* (40 nM) in young and elderly pancreatic sections. Scramble-RNA was negative reference (40 nM), and U6 was positive reference (0.1 nM). The dotted line indicates islet, and the solid line is exocrine. $n = 3$ independent experiments. **D** Representative images of immunofluorescence staining of MKNK1 (green) and amylase (red) in pancreatic sections from young and elderly people and quantitation of amylase and MKNK1 mean fluorescence intensity. $n = 10$. **E** Serum amylase assay of the young adult (YA), the elderly adult (EA) and the elderly adult with diabetes (EA + DM). YA group, $n = 65$. EA group, $n = 65$. EA + DM, $n = 30$. **F** *MiR-503* concentration in human serum of YA, EA and EA + DM. YA group, $n = 45$. EA group, $n = 45$. EA + DM, $n = 30$. **G** Correlation analysis of amylase levels of human serum and age. Each point represents one people ($n = 160$). Correlation coefficient (R) and p value from simple linear regression are shown. **H** Correlation analysis of *miR-503* concentration in human serum and serum amylase levels. Each point represents one people ($n = 120$). Correlation coefficient (R) and P value from simple linear regression are shown. Box plots with centerline = median, box = 25th–75th percentile, and whiskers = 5th–95th percentile, outliers = open circles (**A**, **B**, **D**–**F**). Data are means ± SEM. Data were analyzed using unpaired Student's t tests (**A**, **B**, **D**), one-way ANOVA with Tukey test (**E**, **F**) or Correlation analysis (**G**, **H**). Source data are provided as a Source Data file.

obtained from the Jackson Laboratory. *Elastase* (*ELA*)-CreER mice were obtained from Dr. Xianghui Fu (Professor of the West China Hospital, Sichuan University). We then crossed KI mice with *CAG*-CreER, *PDX1*-Cre, *ELA*-CreER, and *RIP2*-Cre mice, respectively, to obtain global inducible (CKI), pancreas-specific (PKI), acinar cell-specific inducible (EKI), and islet β-cell-specific (βKI) overexpressing *miR-503-322* mice. Details on each animal strain are listed in Table S3. EKI or CKI and their litter control mice were injected intraperitoneally with tamoxifen solution, 100 mg/kg, in corn oil, for three consecutive days to induce miR-503-322 overexpression in acinar cells or the whole body, respectively. The control groups used their respective littermates and were genotyped as KI-positive and Cre-negative. All experimental mice were heterozygous except for PKI mice, which included both homozygotes and heterozygotes. *MiR-503* transgenic mice (βTG) and *miR-503-322* global deletion mice (KO) were also generated by GemPharmatech Co, Ltd. Refer to our previous findings for the exact construction workflow[15]. Aged C57BL6/J mice were purchased from GemPharmatech Co, Ltd.

The animals were randomly allocated to experimental groups, at least four per group, not according to genotype to minimize potential confounding factors. Male mice were mostly used in this study, and female mice were also involved to rule out the sex bias, as described in the figure legends. Mice were housed in a temperature- and humidity-controlled environment (23–25 °C, 12-h light/dark cycle, 60–70% humidity) in a specific pathogen-free facility at Nanjing Medical University and provided with free access to commercial rodent chow (Research Diets, D12450J) and tap water. Health was monitored at least weekly by weight, food and water intake, and general assessment of animal activity, panting, and fur condition. Mice were euthanized by CO_2 asphyxiation when met euthanasia criteria.

Adult animals of both genders were used in tamoxifen induction studies. Collected blood serum was used to measure amylase and lipase. The pancreatic tissue was collected and immediately embedded in an optimum cutting temperature compound for hematoxylin and eosin staining, evaluation of necrosis, and immunohistochemistry.

Pancreatic acinar cell experiments

Mouse pancreatic acini were isolated using the standard collagenase digestion protocol[56]. Acini were isolated and left to recover for 30 min at 37 °C before stimulation with the indicated concentrations of caerulein (MCE, Shanghai, China) to assess the secretory capacity. The supernatant for amylase activity was analyzed with a commercial kit (JianCheng Bioengineering Institute, Nanjing, China) and the percentage of amylase secretion was calculated. To visualize trypsinogen activation in acinar cells, freshly prepared acini were loaded with active trypsin enzyme substrate BZiPAR (10 μM) (Invitrogen, America) and incubated for 30 min. For cytoskeletal analysis, pancreatic acini were isolated and incubated with or without caerulein (0.01 μM) for 30 min. At the indicated times, the cells were harvested and stained for F-actin with phalloidin and nuclei. Images were captured and analyzed by a confocal laser scanning microscope (Olympus FV1200). The image fluorescence intensity was analyzed with ImageJ software. For flow cytometry analysis, EVs labeled with PKH67 were co-incubated with freshly isolated acini for 8 h. Following this, the samples were digested into single cells and subsequently analyzed to determine the percentage of FITC-positive cells.

Induction of murine pancreatitis

Caerulein was solubilized in phosphate-buffered saline at a final concentration of 15 mg/mL. Experimental mice were challenged with caerulein (50 mg/kg, intraperitoneal injection, once an hour, six times) to induce AP. Control animals received an equal amount of saline. The parameters of AP were assessed 2 h after the last caerulein treatment. Edema, serum lipase (ElabScience, Wuhan, China), amylase and trypsin activity (JianCheng Bioengineering Institute, Nanjing, China) were analyzed as parameters of pancreatitis. Necrosis and acinar cell damage quantified by morphometry[57]. Tissue damage was quantified using scoring system as describe by Schmidt et al.[43].

Histopathology, immunohistochemistry, and immunofluorescence

Mice were euthanized by CO_2 asphyxiation and tissue was dissected, rinsed in PBS and fixed overnight in 4% paraformaldehyde (Servicebio). Paraffin embedding, serial sectioning, H&E and Masson staining of all samples were commissioned from Servicebio Technologies. After dewaxing and antigen retrieval, the pancreatic paraffinic sections were incubated with primary antibodies overnight at 4 °C. According fluorescent-conjugated secondary antibodies (Proteintech) were used for multiple labeling, and the nuclei were stained with Hoechst 33342 (5 μg/mL) (Sigma-Aldrich). Fluorescent images were visualized by a confocal laser scanning microscope (Olympus FV1200). Immunohistochemistry staining was labeled with a DAB substrate system (BCA Kit) (Gene Tech), and positively labeled cells were captured by a light microscope (Leica, Germany). Quantification was done with at least three mice per group, three sections per mouse (50 μm apart), and at least 10 microscopic fields per section. The antibodies are listed in Table S4.

Pancreatic ductal infusion of adeno-associated viral (AAV) vectors

Pancreatic ductal infusion was performed following the standard surgical protocol[58]. Serotype 2/8 under insulin 2 promoter of HBAAV2/8-insulin 2-scrambled sequence-zsGreen (Ctr) and HBAAV2/8-insulin 2-mmu-miR-503/322-5p-sponge-zsGreen (SP) were provided by the company of Hanheng Biotechnology Co, Ltd. AAV titer of 10^{11}/mL in PBS, 100 μL total volume in 20 g body weight mice was infused at a rate of 6 μL/min. After infusion and suture, surgical mice were placed on a heated pad (37 °C) until full recovery. Ketoprofen (Sigma, k1751) at a dose of 5 mg/kg once per day was given continuously for 3 d for post-

surgery analgesia. Serotype pancreas of PAAV-CMV-MCS-EF1-mNeonGreen-WPRE (Ctr-AAV) and PAAV-CMV-MKNK1-flag-EF1-mNeonGreen-WPRE (MKNK1-AAV) were provided by the company of OBIO Technology Co, Ltd and were administered to mice via intraperitoneal injection. AAV titer of 10^{11}/mL in PBS, 100 μL total volume in 20 g body weight mice.

Locked nucleic acid (LNA)-based in situ hybridization of *miR-503*

Locked nucleic acid-based in situ assay was introduced to detect *miR-503* in human pancreas sections. Double-labeled with carboxyfluorescein (FAM), LNA-enhanced probes including *U6* snRNA control probe, negative scramble-miR control and has-*miR-503* were constructed by QIAGEN. The assay was performed according to the manufacturer's protocol[59]. In short, sample slides were deparaffinized in xylene and ethanol solutions at room temperature (15–25 °C) and digested with Proteinase K reagent for 10 min at 37 °C. After washing, each sample was reacted with 50 μL of hybridization mix (1 nM LNA *U6* snRNA probe, 40 nM double-FAM LNA *miR-503* probe and scramble-miR) in a programmed hybridizer for 1 h. After strictly washing and blocking, the samples were incubated with anti-FAM reagent for 1 h and labeled with alkaline phosphatase substrates for 2 h. The nuclei were labeled with Nuclear Fast Red. All sample slices were visualized by light microscopy.

Islet and β cell-derived EVs isolation and identification

Freshly isolated islets were cultured in serum-EVs-free medium (11.1 mM glucose) for 7 days, with the medium replaced and collected every 24 h. Mouse islets were digested into single cells and treated with FluoZin™-3 (5 μM) (Thermo Fisher Scientific) for 30 min, followed by fluorescence-activated cell sorting to obtain purified β-cells. β-cells were cultured in 0.1 mg/mL poly-D-lysine (Beyotime, China)-coated well plates and EVs-free medium for 3 days and supernatants were collected for enrichment. The culture medium was centrifuged at 300 × *g* for 5 min and then at 3000 × *g* for 20 min to remove cells and other debris, followed by centrifugation at 10,000 × *g* for 30 min to remove large vesicles. Then, the supernatant was centrifuged at 110,000 × *g* for 2 h. EVs were collected from the pellets and resuspended in an FBS-free medium or PBS. All centrifugation steps were performed at 4 °C. For the identification of EVs, TEM, NTA, and Western blot analyses were performed. For TEM, EVs were fixed overnight at 4 °C in a droplet of 2.5% glutaraldehyde in PBS (pH 7.2). The samples were then washed with PBS three times (10 min each) and post-fixed in 1% osmium tetroxide for 60 min at room temperature. Samples were then embedded in 10% gelatin, fixed in glutaraldehyde at 4 °C, cut into several blocks (<1 mm^3 in volume), and dehydrated for 10-min dehydration steps in alcohol at increasing concentrations (30%, 50%, 70%, 90%, 95%, and 100% × 3). Pure alcohol was then replaced with propylene oxide, and the samples were infiltrated with Quetol 812 epoxy resin at increasing concentrations (25%, 50%, 75%, and 100%) with propylene oxide for a minimum of 3 h per step. Next, the samples were embedded in 100% fresh Quetol 812, polymerized at 35 °C for 12 h, and then at 60 °C for 24 h. Ultrathin sections (100 nm) were obtained from the prepared samples using a Leica UC6 ultramicrotome. Finally, the samples were post-stained with uranyl acetate for 10 min and lead citrate for 5 min at room temperature and observed using an FEI Tecnai T20 TEM operated at 120 kV. NTA was performed using a NanoSight NS300 system (NanoSight), which focuses a laser beam through a suspension of the particle of interest. The results were visualized by light scattering. For western blotting, ALIX, TSG101, and CD63 were used as markers for nano-vesicles and GAPDH was used as a negative control. For cell imaging, EVs were labeled with PKH67 (Sigma-Aldrich) for 1 h and then washed three times with PBS. PKH67-labeled EVs (6e + 5 particles/35 mm culture dish) were resuspended in PBS and then incubated with freshly isolated acini for 8 h. The acini were then stained with phalloidin (MCE) for 15 min and Hoechst 33342 for 8 min. Images were taken and analyzed by a confocal laser scanning microscope (Olympus FV1200).

Plasmid construction and dual-luciferase reporter assay

The WT and mutant 3′ UTR-luciferase constructs containing *miR-503-322* binding site of mouse *Mknk1* were generated by annealing and cloning the short sequences into pMIR-REPORT Luciferase miRNA Expression Reporter Vector (Ambion) between the SpeI and HindIII sites. Primer sequences are listed in Table S5. Luciferase activities were measured using the Dual-Glo Luciferase Assay System (Promega, America) on a TD-20/20 Luminometer (Turner BioSystems, America) according to the manufacturer's protocols.

Quantitative RT-PCR

Total RNA was extracted from cells and tissues using Trizol reagent (Invitrogen). cDNA was synthesized from total RNA using a ReverTra Ace Kit (TOYOBO, Japan). qPCR of Pri-miRNA and miRNA were performed using the THUNDERBIRD probe qPCR Mix (TOYOBO, Japan), and SYBR Green qPCR Master Mix (Vazyme, China) for mRNA on Roche LightCycle480 II Sequence Detection System (Roche, Switzerland). Primers of qPCR for pri-miRNA and miRNA were purchased from Thermofisher Co., Ltd, other primer sequences were available in Table S5.

Western blot analysis

Cells or tissues were lysed with ice-cold RIPA buffer (Thermo Fisher Scientific), supplemented with 0.5 mM EDTA and Halt protease/phosphatase inhibitor cocktail (Thermo Fisher Scientific), rotated at 4 °C for 15–30 min to mix, and centrifuged at maximum speed for 15 min to collect whole cell lysates. Protein concentration was measured with the BCA protein assay (Takara). Thirty mg of total protein per sample was loaded into 4–12% NuPAGE Tris-Bis (Thermo Fisher Scientific) gradient gels and separated by SDS-PAGE. Proteins were transferred to PVDF membranes (Millipore Billerica) and blocked with 5% milk. Beta-actin and α-tubulin were used as loading controls. Primary antibodies were detected with HRP-conjugated (Sigma-Aldrich) secondary antibodies for chemiluminescent detection (Perkin Elmer ECL). Protein quantification was performed by ImageJ (NIH Image). Key reagents and antibodies are listed in Table S6.

Statistical analysis

All results were expressed as mean ± SEM. Results were analyzed with GraphPad Prism software (version 8.3.0, San Diego, CA, USA). Two-tailed unpaired Student's *t* test was used for the comparison of two sets. Differences in means between multiple groups were analyzed by ordinary one-way analysis of variance followed by Tukey's multiple comparisons. Two-way ANOVA followed by Tukey's multiple comparisons was used for two-way analysis. Linear regression analysis was performed using GraphPad Prism software. Pearson correlation analysis was used to test for correlations. In all analyses, $P < 0.05$ was considered statistically significant.

Reporting summary

Further information on research design is available in the Nature Portfolio Reporting Summary linked to this article.

Data availability

The source data generated in this study are provided in the Source Data file. This paper does not report the original code. Any additional information is available upon request to the corresponding author (Yunxia Zhu, zhuyx@njmu.edu.cn). Source data are provided with this paper.

References

1. Baeza-Zapata, A. A., Garcia-Compean, D. & Jaquez-Quintana, J. O. & Collaborators. Acute pancreatitis in elderly patients. *Gastroenterology* **161**, 1736–1740 (2021).
2. Kayar, Y., Dertli, R. & Konur, S. Clinical outcomes of acute pancreatitis in elderly patients: an experience of single tertiary center. *Pancreatology* **20**, 1296–1301 (2020).
3. Satis, H., Kayahan, N., Sargin, Z. G., Karatas, A. & Celiker, D. Evaluation of the clinical course and prognostic indices of acute pancreatitis in elderly patients: a prospective study. *Acta Gastroenterol. Belg.* **83**, 413–417 (2020).
4. Grunewald, M. et al. Counteracting age-related VEGF signaling insufficiency promotes healthy aging and extends life span. *Science (New York, N.Y.)* **373**, https://doi.org/10.1126/science.abc8479 (2021).
5. Investigators, F. S. Effects of long-term fenofibrate therapy on cardiovascular events in 9795 people with type 2 diabetes mellitus (the FIELD study): randomised controlled trial. *Lancet* **368**, 1420–1420 (2006).
6. Girman, C. J. et al. Patients with type 2 diabetes mellitus have higher risk for acute pancreatitis compared with those without diabetes. *Diab. Obes. Metab.* **12**, 766–771 (2010).
7. Gonzalez-Perez, A., Schlienger, R. G. & Rodriguez, L. A. Acute pancreatitis in association with type 2 diabetes and antidiabetic drugs: a population-based cohort study. *Diab. Care* **33**, 2580–2585 (2010).
8. Mizumoto, R. & Sakoguchi, T. Relationship between endocrine and exocrine glands of the pancreas. *Nihon Rinsho. Jpn. J. Clin. Med.* Suppl, 2250–2251 (1978).
9. Williams, J. A. & Goldfine, I. D. The insulin-pancreatic acinar axis. *Diabetes* **34**, 980–986 (1985).
10. Barreto, S. G., Carati, C. J., Toouli, J. & Saccone, G. T. The islet-acinar axis of the pancreas: more than just insulin. *Am. J. Physiol. Gastrointest. Liver Physiol.* **299**, G10–22, (2010).
11. Chung, K. M. et al. Endocrine-exocrine signaling drives obesity-associated pancreatic ductal adenocarcinoma. *Cell* **181**, 832 (2020).
12. Schludi, B. et al. Islet inflammation and ductal proliferation may be linked to increased pancreatitis risk in type 2 diabetes. *JCI Insight.* **2**, https://doi.org/10.1172/jci.insight.92282 (2017).
13. Li, X. et al. Islet alpha-cell inflammation induced By NF-kappaB inducing kinase (NIK) leads to hypoglycemia, pancreatitis, growth retardation, and postnatal death in mice. *Theranostics* **8**, 5960–5971 (2018).
14. Li, J. et al. Pancreatic beta cells control glucose homeostasis via the secretion of exosomal miR-29 family. *J. Extracell. Vesicles* **10**, e12055 (2021).
15. Zhou, Y. et al. β-Cell miRNA-503-5p induced by hypomethylation and inflammation promotes insulin resistance and β-cell decompensation. *Diabetes* **73**, 57–74 (2024).
16. Liang, R. et al. H19X-encoded miR-322(424)/miR-503 regulates muscle mass by targeting translation initiation factors. *J. Cachexia Sarcopenia Muscle* **12**, 2174–2186 (2021).
17. Aguayo-Mazzucato, C. et al. Acceleration of beta cell aging determines diabetes and senolysis improves disease outcomes. *Cell Metab.* **30**, 129–142.e124 (2019).
18. Jayaraman, S. A novel method for the detection of viable human pancreatic beta cells by flow cytometry using fluorophores that selectively detect labile zinc, mitochondrial membrane potential and protein thiols. *Cytom. A* **73**, 615–625 (2008).
19. Hermann, P. C. et al. Nicotine promotes initiation and progression of KRAS-induced pancreatic cancer via Gata6-dependent dedifferentiation of acinar cells in mice. *Gastroenterology* **147**, 1119–1133.e1114 (2014).
20. Weidemann, B. J. et al. Repression of latent NF-kappaB enhancers by PDX1 regulates beta cell functional heterogeneity. *Cell Metab.* **36**, 90–102.e107 (2024).
21. Jiang, Z. E. et al. Age-associated changes in pancreatic exocrine secretion of the isolated perfused rat pancreas. *Lab Anim. Res.* **29**, 19–26, (2013).
22. Chvanov, M. et al. Intracellular rupture, exocytosis and actin interaction of endocytic vacuoles in pancreatic acinar cells: initiating events in acute pancreatitis. *J. Physiol.* **596**, 2547–2564 (2018).
23. Sendler, M. et al. Cathepsin B-mediated activation of trypsinogen in endocytosing macrophages increases severity of pancreatitis in mice. *Gastroenterology* **154**, 704–718.e710 (2018).
24. Desai, B. M. et al. Preexisting pancreatic acinar cells contribute to acinar cell, but not islet beta cell, regeneration. *J. Clin. Invest.* **117**, 971–977 (2007).
25. Cendrowski, J. et al. Mnk1 is a novel acinar cell-specific kinase required for exocrine pancreatic secretion and response to pancreatitis in mice. *Gut* **64**, 937–947 (2015).
26. Hardt, P. D. et al. Pancreatic exocrine function in patients with type 1 and type 2 diabetes mellitus. *Acta Diabetol.* **37**, 105–110 (2000).
27. Yilmaztepe, A., Ulukaya, E., Ersoy, C., Yilmaz, M. & Tokullugil, H. A. Investigation of fecal pancreatic elastase-1 levels in type 2 diabetic patients. *Turk. J. Gastroenterol.* **16**, 75–80 (2005).
28. Yatchenko, Y., Horwitz, A. & Birk, R. Endocrine and exocrine pancreas pathologies crosstalk: insulin regulates the unfolded protein response in pancreatic exocrine acinar cells. *Exp. Cell Res.* **375**, 28–35 (2019).
29. Solanki, N. S., Barreto, S. G. & Saccone, G. T. P. Acute pancreatitis due to diabetes: the role of hyperglycaemia and insulin resistance. *Pancreatology* **12**, 234–239 (2012).
30. Hardt, P. D. et al. Chronic pancreatitis and diabetes mellitus. A retrospective analysis of 156 ERCP investigations in patients with insulin-dependent and non-insulin-dependent diabetes mellitus. *Pancreatology* **2**, 30–33 (2002).
31. Majumder, S. et al. Diabetes mellitus is associated with an exocrine pancreatopathy (EP) that is distinct from chronic pancreatitis (CP). *Pancreas* **44**, 1395–1395 (2015).
32. Zechner, D. et al. Diabetes aggravates acute pancreatitis and inhibits pancreas regeneration in mice. *Diabetologia* **55**, 1526–1534 (2012).
33. Zechner, D. et al. Diabetes increases pancreatic fibrosis during chronic inflammation. *Exp. Biol. Med.* **239**, 670–676 (2014).
34. Rupnik, M. S. & Hara, M. Local dialogues between the endocrine and exocrine cells in the pancreas. *Diabetes*, **73**, 533–541 (2024).
35. Whitcomb, D. C., Buchner, A. M. & Forsmark, C. E. AGA clinical practice update on the epidemiology, evaluation, and management of exocrine pancreatic insufficiency: expert review. *Gastroenterology* **165**, 1292–1301 (2023).
36. Kudoh, A., Katagai, H., Takazawa, T. & Matsuki, A. Plasma proinflammatory cytokine response to surgical stress in elderly patients. *Cytokine* **15**, 270–273 (2001).
37. Barbeiro, D. F., Koike, M. K., Coelho, A. M. M., da Silva, F. P. & Machado, M. C. C. Intestinal barrier dysfunction and increased COX-2 gene expression in the gut of elderly rats with acute pancreatitis. *Pancreatology* **16**, 52–56 (2016).
38. Kim, C. I. Clinicopathological study of pancreatic fibrosis in diabetes mellitus. *Med. J. Osaka Univ.* **28**, 23–31 (1977).
39. Lohr, J. M., Panic, N., Vujasinovic, M. & Verbeke, C. S. The ageing pancreas: a systematic review of the evidence and analysis of the consequences. *J. Intern. Med.* **283**, 446–460 (2018).
40. Sato, T. et al. Age-related changes in normal adult pancreas: MR imaging evaluation. *Eur. J. Radiol.* **81**, 2093–2098 (2012).
41. Banks, P. A. et al. Classification of acute pancreatitis-2012: revision of the Atlanta classification and definitions by international consensus. *Gut*. **62**, 102–111 (2013).
42. Kleeff, J. et al. Chronic pancreatitis. *Nat. Rev. Dis. Prim.* **3**, 17060 (2017).

43. Schmidt, J. et al. A better model of acute pancreatitis for evaluating therapy. *Ann. Surg.* **215**, 44–56 (1992).
44. Shen, X. et al. miR-322/-503 cluster is expressed in the earliest cardiac progenitor cells and drives cardiomyocyte specification. *Proc. Natl. Acad. Sci. USA* **113**, 9551–9556 (2016).
45. Wang, G. et al. Tumour extracellular vesicles and particles induce liver metabolic dysfunction. *Nature* **618**, 374–382 (2023).
46. Li, K. et al. Salivary extracellular MicroRNAs for early detection and prognostication of esophageal cancer: a clinical study. *Gastroenterology* **165**, 932–945 e939 (2023).
47. Jiang, T. Y. et al. PTEN deficiency facilitates exosome secretion and metastasis in cholangiocarcinoma by impairing TFEB-mediated lysosome biogenesis. *Gastroenterology* **164**, 424–438 (2023).
48. Wang, J. et al. Extracellular vesicles mediate the communication of adipose tissue with brain and promote cognitive impairment associated with insulin resistance. *Cell Metab.* **34**, 1264–1279.e1268 (2022).
49. Cao, M. et al. Cancer-cell-secreted extracellular vesicles suppress insulin secretion through miR-122 to impair systemic glucose homeostasis and contribute to tumour growth. *Nat. Cell Biol.* **24**, 954–967 (2022).
50. Li, S. et al. Hair follicle-MSC-derived small extracellular vesicles as a novel remedy for acute pancreatitis. *J. Control. Release* **352**, 1104–1115 (2022).
51. Hu, Z. et al. MSCs deliver hypoxia-treated mitochondria reprogramming acinar metabolism to alleviate severe acute pancreatitis injury. *Adv. Sci.* **10**, e2207691 (2023).
52. Ryaboshapkina, M. et al. Characterization of the secretome, transcriptome, and proteome of human beta cell line EndoC-betaH1. *Mol. Cell Proteom.* **21**, 100229 (2022).
53. Midha, A. et al. Unique human and mouse beta-cell senescence-associated secretory phenotype (SASP) reveal conserved signaling pathways and heterogeneous factors. *Diabetes* **70**, 1098–1116 (2021).
54. Saluja, A., Dudeja, V., Dawra, R. & Sah, R. P. Early intra-acinar events in pathogenesis of pancreatitis. *Gastroenterology* **156**, 1979–1993 (2019).
55. Kim, Y. A. et al. Severe acute pancreatitis due to tamoxifen-induced hypertriglyceridemia with diabetes mellitus. *Chin. J. Cancer Res.* **26**, 341–344, (2014).
56. Grosfils, K., Metioui, M., Tiouli, M. & Dehaye, J. P. Isolation of rat pancreatic acini with crude collagenase and permeabilization of these acini with streptolysin O. *Res. Commun. Chem. Pathol. Pharmacol.* **79**, 99–115 (1993).
57. Bhatia, M. et al. Role of substance P and the neurokinin 1 receptor in acute pancreatitis and pancreatitis-associated lung injury. *Proc. Natl Acad. Sci. USA* **95**, 4760–4765 (1998).
58. Xiao, X. et al. Pancreatic cell tracing, lineage tagging and targeted genetic manipulations in multiple cell types using pancreatic ductal infusion of adeno-associated viral vectors and/or cell-tagging dyes. *Nat. Protoc.* **9**, 2719–2724 (2014).
59. Obernosterer, G., Martinez, J. & Alenius, M. Locked nucleic acid-based in situ detection of microRNAs in mouse tissue sections. *Nat. Protoc.* **2**, 1508–1514 (2007).

Acknowledgements

We are indebted to Scribendi Inc. (Chatham, ON, Canada) for proof-reading the manuscript. This work was supported by grants from the National Natural Science Foundation of China (82330027 to X.H.; 82470840, 82270844, and 82070843 to Y.-X.Z.; 82401002 to K.-R.L.) and Wuxi Science and Technology Development Fund (K20231061 to K.-R.L.).

Author contributions

Conceptualization: Y.-X.Z., X.H. and L.L.; methodology: K.-R.L., T.-T.L., L.H., Y.Z. and X.X; investigation: Y.Z., L.H., W.T. and S.-S.W.; visualization: K.-R.L. and Y.-X.Z.; supervision: Y.Z., Y.-T.L., and X.-A.C.; writing—original draft: K.-R.L. and Y.-X.Z.; writing—review & editing: K.-R.L., X.H., S.-J.P. and Y.-X.Z.; funding acquisition: X.H., Y.-X.Z. and K.-R.L. All authors discussed the results and commented on the manuscript.

Competing interests

The authors declare no competing interests.

Additional information

Supplementary information The online version contains supplementary material available at https://doi.org/10.1038/s41467-025-57615-x.

Correspondence and requests for materials should be addressed to Stephen J. Pandol, Ling Li, Xiao Han or Yunxia Zhu.

Peer review information *Nature Communications* thanks Naziruddin Bashoo and the other anonymous reviewer(s) for their contribution to the peer review of this work. A peer review file is available.